Scientia Iranica B (2021) 28(3), 1284–1297

Sharif University of Technology
Scientia Iranica
Transactions B: Mechanical Engineering
http://scientiairanica.sharif.edu

An experimental investigation of the effect of using non-Newtonian nanofluid–graphene oxide/aqueous solution of sodium carboxymethyl cellulose–on the performance of direct absorption solar collector

V. Sadeghi[a,*], S. Baheri Islami[a], and N. Arsalani[b]

a. *Department of Mechanical Engineering, University of Tabriz, Tabriz, Iran.*
b. *Research Laboratory of Polymer, Department of Organic and Biochemistry, Faculty of Chemistry, University of Tabriz, Tabriz, Iran.*

Received 10 December 2019; received in revised form 29 March 2020; accepted 8 June 2020

KEYWORDS
Non-Newtonian base fluid;
Graphene oxide nanoparticle;
Direct absorption solar collector;
Efficiency;
Extinction coefficient.

Abstract. To improve the performance of Direct Absorption Solar Collectors (DASCs), high photo-thermal potential in nanofluids has always been of interest to researchers. Therefore, the present study mainly aimed to use Graphene Oxide (GO) nanofluids due to their high optical absorption capability and excellent dispersion stability. The novelty of this study is the investigation of the special capability of the optical properties of GO and the thermal potential of non-Newtonian shear-thinning nanofluids together for improving the photo-thermal conversion performance of the DASC model. For this purpose, non-Newtonian and Newtonian nanofluids, involving GO nanoparticles, dispersed in sodium carboxymethyl cellulose (Na-CMC) and deionized water as a base fluid, respectively, were prepared and experimentally tested. The flow rate, weight percentage and incident radiation have been selected as test parameters for estimating the efficiency of the collector. The results showed that the efficiency improved by increasing the weight percentage of nanoparticles in both nanofluids. Furthermore, by changing the base fluid from Newtonian to non-Newtonian, the reduction in efficiency at 0.01 wt% was by (9.4–15.63)% and at 0.03 wt% was by (19.84–26.46)%. Additionally, GO nanofluid sample (S_3) was found appropriate for the designed DASC model due to its optimum efficiency and temperature difference rise rate.

1. Introduction

The factors such as increasing global demand for energy and dependence on fossil fuels had many harmful effect on the environment and caused major challenges to be created including global warming, greenhouse gas emissions, and environmental degradation. Among the sources of renewable energies, solar energy is one of the most useful and available energy resources due to various applications such as heat, electricity, and light [1–3]. The use of nanofluids to increase the rate of heat transfer in solar and non-solar energy systems has always been of interest [4]. The non-solar aspects of nanofluids had been the subject of some studies, in this regard the study performed by Li et al. [4] can be

*. *Corresponding author. Tel.: +984133803727*
E-mail address: v-sadeghi@tabrizu.ac.ir (V. Sadeghi)

doi: 10.24200/sci.2020.54994.4024

referred to. They showed that two factors of Brownian motion and thermophoresis will improve heat transfer. Sheikholeslami et al. [5] also reported an increase in boiling heat transfer by using nanofluid and flattening tube. On the other hand, important applications of nanofluids in solar energy systems include [6]: Solar collectors, photovoltaic-thermal (PV/T) systems, power systems, thermal energy storage, solar thermoelectric devices and etc. Solar collectors which are widely-used as thermal systems, provide an effective way to collect or concentrate solar radiation [6,7]. This research is directed towards the efficient collection of high quality thermal energy from the incident radiation energy. Since flat plate solar collectors have offered limited efficiency and low output temperatures due to heat loss [5–8], improving the thermal performance of solar collectors through effective parameters (e.g. working fluid) has always received attention from many researchers. Moreover, direct absorption volume collectors with suitable nanofluids have been investigated and proposed as an alternative by researchers. Nanofluids are a relatively new class of fluids that act as a promising alternative to conventional fluids in a Direct Absorption Solar Collector (DASC) due to their unique optical properties. Nanofluids are nanotechnology-based heat transfer fluids that are engineered by stably-dispersing nano-sized solid particles in conventional heat transfer fluids at relatively low particle volume concentrations [8]. The nanoparticle suspensions are assumed as effective electromagnetic wave absorbers within UV-Visible wavelength ranges where 85% of solar energy falls within the range of 280–1200 nm. In this regard it is worthy of consideration that the conventional fluids absorb 15% of solar energy falls within the spectrum 1200–2500 nm [9,10]. Nanoparticles are considered the basis of thermal applications due to their unique optical and thermal properties [10]. The graphene nanoparticles received more attention than other nanoparticles because of their specific advantages over their counterparts and their application in the field of engineering came to be considered by researchers [11]. These advantages include the following:

- Higher thermal conductivity;
- Higher heat transfer capability;
- Being more stable than other nanoparticles;
- Excellent optical absorption properties;
- Better photo-thermal conversion performance.

It should be noted that nanofluids have been considered as an efficient heat transfer fluids for nearly two decades which could be used for enhancing the performance of thermal systems, especially solar collectors. Minardi and Chung [12] first explored the concept of solar absorber solar collectors in 1970, resulting in lower thermal losses and improved thermal performance compared to conventional surface collectors. In this regard, some studies have been conducted on DASCs with multiple nanofluids including graphene based nanofluids. Numerical and experimental simulation results obtained by Luo et al. [13] were applicable for different nanofluids in DASC. Compared to the base fluid, the nanofluids under discussion, improved the outlet temperature from 30 to 100 K and the efficiency from 2% to 25%. Further, the photothermal efficiency of graphite nanofluid was reported 122.7% at a volume fraction of 0.01%. Liu et al. [14] experimentally and numerically studied graphene nanofluids in ionic liquid in DASC. They reported the receiver efficiency increases with the solar intensity and receiver height, but decreases with the graphene concentration. They also obtained the efficiency of the receiver equal to 70% at a weight percentage of 0.0005 wt% under the conditions of the receiver of 5 cm and radiation flux of 20 kW/m^2. In two experimental studies on graphene nanofluids in volume solar collector, conducted by Vakili et al. [15] (that was the first one conducted for the home water heater system) the efficiency at weight percentages of 0.0005 wt%, 0.001 wt%, and 0.005 wt% were 83.5%, 89.7%, and 93.2%, respectively. Furthermore, another study [16] was conducted on the direct absorption collector with the low temperature model at the weight percentages of 0.00025 wt%, 0.0005 wt%, 0.001 wt%, and 0.005 wt%. They indicated that graphene nanofluids were proper for these types of collectors because of their strong absorption in the range of 250–300 nm. Khosrojerdi et al. [17] reported the experimental evaluation of (GO/water) nanofluids at weight percentages of 0.001 wt%, 0.005 wt%, 0.015 wt% and 0.045 wt%, concluding the absorption of 96.6% energy at weight percentage of 0.045 wt% and height of 3 cm. Chen et al. [18] conducted an experimental study to improve the performance of DASCs with Reduced Graphene Oxide (RGO) nanofluid. They obtained the photo thermal efficiency equal to 52% and 96.33% at temperatures of 30°C and 75°C, respectively. Ma et al. [19] demonstrated the encapsulation efficiency of 37.93% for the manufacture of novel slurry containing Graphene Oxide (GO) modified with paraffin @titania(TiO_2)/GO micro-capsule for DASC. Also, Campos et al. [20] investigated the effect of the relationship between particle shape and GO on the behavior of DASCs with metal-based nanofluid, GO, and GO/silver composite structures. They showed an increase in the efficiency of spherical metal nanofluids by about 35% compared to the pure water-based fluid. Moreover, an increase in the efficiency by 20% was observed for non-spherical silver particles in the GO/silver composite structure compared to the spherical silver nanofluid state. Xu et al. [21] carried out an experimental-numerical study with the (RGO/water-EG) nanofluid as the working

fluid on direct absorption collector. They showed an increase in the temperature by 76.9% and efficiency by 70% compared to the base fluid.

Recent studies have shown that improving the photo-thermal conversion performance of DASCs is often accomplished through two methods of increasing the absorption coefficient and changing the working fluid heat transfer mechanism in the collector chamber. Here are some of the most serious and recent research in this area. Gorji and Ranjbar [22] provided a summary report on the recent developments and researches on the optical properties and application of nanofluids in DASCs. They also described the approaches and challenges facing DASCs researches and then made some proposals in this context. Mallah et al. [10] employed plasmonic nanofluids based on noble metal nanoparticles as well as controlling absorption and spectral scattering coefficients for improving the photo-thermal conversion efficiency. According to the results, these types of nanofluids exhibited high performance in low volume fractions of the broadband solar spectrum. The photo-thermal conversion properties of magnetic nanoparticles through a rotating magnetic field in DASCs were investigated by Wang et al. [23]. They changed the heat transfer mechanism from conduction to convection, showing that the photo-thermal conversion efficiency for the Fe Ni/C-EG nanofluid is 58.1%. This represents a 22.7% improvement in comparison with the magnetic field without external rotation at 50 ppm nanoparticles. In another study [24], they investigated the photo-thermal conversion efficiency of the binary nanofluids (α-Fe_2O_3-GO/EG) in the new system. The results showed that the photo-thermal conversion efficiency for this nanofluid reached up to 56.8%. This represents a 14.5% increase over magnetic nanofluids without external rotation for the RGO content of 0.007 wt%. The study of two functionalized graphene nanofluids including hydroxylated graphene (GOH) and carboxylated graphene (GO-COOH) with EG-water base fluid was conducted by Huang et al. [25]. The results showed that at a radiant flux of 1000 W/m^2 the final temperature of nanofluid (GOH/EG-water) reaches 55°C at 0.007 wt%. In addition, due to the significant dispersion stability characteristic at high temperatures, this fluid is a promising fluid for use in low temperature DASCs. Sharaf et al. [26] studied ultra-stable plasmonic nanofluids using citrate- (CIT-) and polyethylene glycol-coated (PEG-) gold nanoparticles in optimum solar collectors to investigate the long-term stability of nanofluids in the storage process. The results showed that these materials exhibited excellent electrosteric stabilization, superior colloidal stability, and more compatible optical properties. Hazra et al. [27] increased the photo-thermal conversion efficiency of carbon black-ethylene glycol nanofluids by approximately 27.9% compared to the sole ethylene glycol, using 15 ppm carbon black-ethylene glycol nanofluids for a duration of 1200 seconds. Wang et al. [28] analyzed the photo-thermal conversion efficiency of nanofluids using reverse illumination method by the Rayleigh-Benard convection transfer mechanism on the DASCs. According to the results, the efficiency increased by 51.9% in comparison with conventional DASCs. The application of artificial neural networks to predict the performance of the DASCs based on nanofluids was studied by Delfani et al. [29]. According to the results, changing the collector depth from 5 to 15 mm results in an increase in collector efficiency by about 9%. In addition, the Nusselt number of the collector increases substantially with the collector depth and nanofluid flow rate. Wang et al. [30] examined the photo-thermal performance evaluation on multi-walled carbon nanotubes (MWCNTs)-dispersed Microencapsulated Phase Change Materials (MPCMs) slurries for DASCs. Their reports indicated that the final increase in temperature of the hybrid solution containing 15 wt% MPCMs is about 4.6°C. Improvement in the thermal performance of the industrial heating and cooling systems can be achieved by taking advantage of the non-Newtonian characteristics of nanofluids [31]. Numerous studies have recently been conducted on the thermal capability of non-Newtonian nanofluids. The special attention has been paid to the study of non-Newtonian nanofluids based on Na-CMC, known as well-dispersed fluid. Some examples of researches in this area are as follows : Hojjat et al. [32] experimentally investigated the forced convection heat transfer of the three different types of non-Newtonian nanofluids by homogeneously dispersing Al_2O_3, TiO_2, and CuO nanoparticles. In this study an aqueous solution with 0.5 wt% CMC was used as the base fluid. The results showed that the thermal conductivity of the nanofluids was higher than the base fluid and increased with increasing temperature. Also, a comparison of the heat transfer coefficient of the Newtonian and non-Newtonian fluids in the laminar fluids passing through spiral tube coils conducted by Pimenta and Campos [33] showed that for the same Prandtl numbers, the Nusselt number of the CMC solutions is generally higher than the Newtonian fluids. Sharifi Asl et al. [34] numerically investigated the heat transfer coefficient of non-Newtonian nanofluids inside a tube. Based on the results, the heat transfer coefficient and the Nusselt number of the non-Newtonian alumina-CMC increased compared to the non-Newtonian base fluid. Moreover, they reported that by changing the rheological behavior of fluid from Newtonian to non-Newtonian states the convective heat transfer coefficient of the base fluid could be improved considerably. The effect of velocity and dimension of solid nanoparticles on the heat transfer of non-Newtonian nanofluid containing alumina nanoparticles with the volume fraction of 0.5%

and 1.5% and CMC with 0.5 wt% was investigated by Akbari et al. [35]. The results showed that increasing the volume fraction of solid nanoparticles and decreasing the nanoparticle diameter improves heat transfer. Shamsi et al. [36] studied the heat transfer of non-Newtonian Al_2O_3/CMC nanofluids in a rectangular micro-channel with triangular ribs. Based on the results, heat transfer increased with increasing volume fraction and decreasing nanoparticle diameter. In another study, the use of experimental data to estimate heat transfer and pressure drop of non-Newtonian nanofluid flow through a circular tube was investigated by Shahsavani et al. [37]. According to the results, the heat transfer coefficient increased by 44% at 1% volume fraction and 50°C. Finally, in a slightly different study, Siddiqa et al. [38] analyzed the radiative heat transfer from a non-Newtonian dusty Casson fluid flow along a complex wavy surface. As revealed by the results of this study, when the radiation parameter and mass concentration parameter affected the mechanism, the heat transfer rate increased significantly. This increase reflects the significant role of non-Newtonian fluid flow and heat transfer characteristics in engineering applications.

Based on previous researches, the aqueous solution of Na-CMC was employed in this study. This fluid is well-known as a non-Newtonian quasi-plastic fluid and is capable of improving heat exchange rate and dispersing ability in the water. In previous studies, the use of non-Newtonian nanofluids as a working fluid has not been investigated in DASCs, which seems to be an appropriate option in these collectors in dilute fluid mode due to the need for low pumping power. Moreover, the radiation properties of non-Newtonian nanofluids have not been measured and evaluated for use in collectors. Therefore, the Newtonian and non-Newtonian nanofluids were selected by dispersing GO and RGO nanoparticles, respectively, in the base fluid of deionized water and Na-CMC with various content. Among the studies conducted in this field, the effect of weight percentage and flow rate on the photo-thermal conversion performance of the designed DASC model is worthy of consideration. The aim of this study is to investigate the effects of low effective viscosity non-Newtonian quasi-plastic base fluid by examining the radiative properties of the working fluid to improve the fluid heat transfer coefficient. Also, its combination with GO nanoparticles, including the superior advantages of appropriate photo-thermal properties and high thermal conductivity, as well as good dispersion stability, make suitable working fluid for using in DASC. Moreover, the optical and thermophysical properties of the non-Newtonian nanofluids were compared with the Newtonian fluid under similar conditions, and the influence of these parameters on the model efficiency was also discussed. The main novelty of this study lies in the fact that to improve the efficiency of the DASC model, the effects of the optical properties of GO nanofluids and the thermal potential of non-Newtonian nanofluids was studied simultaneously.

2. Experimental setup

2.1. Setup specification

The model dimensions, presented in this study were inspired by the work of Gorji and Ranjbar [39] who designed the direct absorption collector. The main sections of the experimental set-up are schematically depicted in Figure 1.

In the circulation cycle of the model, the prepared

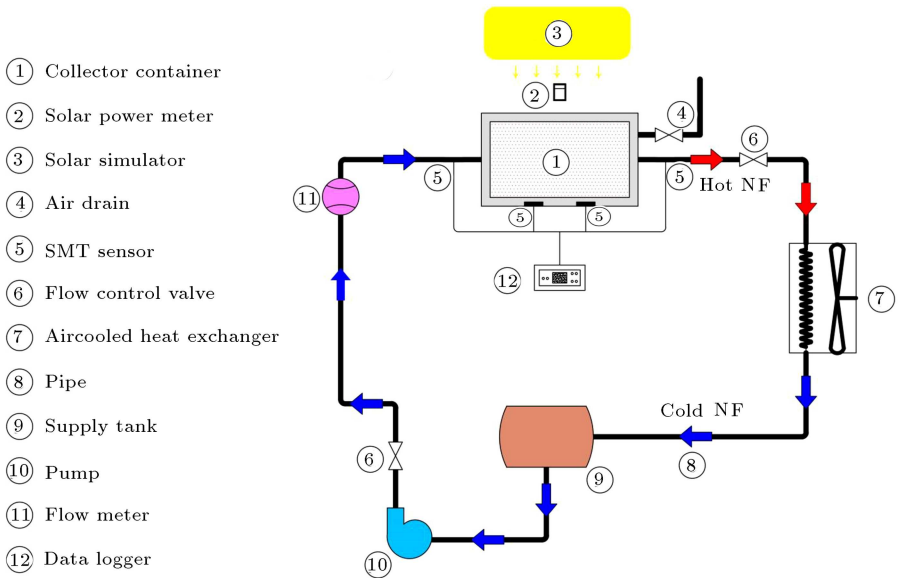

Figure 1. Schematic of the experimental setup.

nanofluid sample flowed into the collector container–after entering the supply tank–via a pump and by adjusting the flow rate through the flow control valve. The rectangular collector container has been made of Al7000 reflex aluminum with the dimensions of 13 cm in length, 6 cm in width, and 2.5 cm in height and its body was insulated with expandable polystyrene foam with the thickness of 4 cm and thermal conductivity coefficient of 0.036 W/m. Moreover, an air vent was prescribed in the collector container to evacuate the air. Furthermore, the glass was used with a thickness of 3 mm and a transmissivity of 0.92. Four SMT160-30B12A temperature sensors (with the absolute accuracy of $\pm 0.7^{\circ}$C) were used to measure the collector working fluid temperature – one sensor was installed in the chamber inlet, two sensors in the middle part of the chamber, and one sensor in the collector output part. The collector working fluid temperature was recorded every 20 seconds by the installed sensors using a data logger and the ambient temperature was measured by a thermometer with a precision of 0.2%. (Average ambient temperature of the laboratory is $T_{amb} = 16^{\circ}$C) To adjust the flow rate of the collector system, a TGI flowmeter with an accuracy of 4% in the range of 6 to 60 ml/min was used. Moreover, the experimental test on volume flow rates of nanofluids was performed for three modes, including 20, 40, and 60 ml/min. These flow rates were selected to allow the flowing fluid to achieve the measurable temperature rises and also to attain the steady state conditions. The calibration of the volume flow rate was done by drawing off and pumping water into a graduated cylinder and measuring the time with an accurate stopwatch. To simulate the solar spectrum, an Osram metal halide lamp (HQI 1000 W/D) with a color temperature of 7250K was used that radiated perpendicular to the collector plate. The lamp was illuminated after the fluid flow reached the steady state in the system. The measured incident radiation varied from 664 to 1938 W/m^2 when the height of the lamp was maintained at 15 cm above the collector. The mentioned radiation range has been selected to allow the appropriate absorption of incident radiation for the flowing fluid while maintaining steady state conditions within ± 10 W/m^2. The TES1333 solar power meter was used with an accuracy of 5% to measure incident radiation flux. After the fluid was exited from the collector chamber, it was cooled by an air-cooled heat exchanger, then it entered the supply tank to complete the system flow cycle.

2.2. Uncertainty analysis

In this experiment, the calibration process of measuring instruments was performed using calibrated references. The uncertainty components affecting the collector thermal efficiency were collector thermal efficiency were inaccuracy in temperature measurement, volume flow rate measurement, and intensity of incident radiation measurement The general uncertainty analysis was assessed by using the following equation [40]:

$$U_r^2 = \sum_{j=1}^{n} U_{xj}^2, \tag{1}$$

where U_r stands for the general uncertainty of the measurement parameter and U_{xj} is the Root Sum Square (RSS) of scattering and measuring the uncertainty of each measured parameter.

The instantaneous collector efficiency was obtained from the following relation:

$$\eta = \frac{\rho \dot{V} C_P (T_o - T_i)}{G_T A_c}, \tag{2}$$

where $\dot{V}$ is the volume flow rate, ρ is nanofluid density, C_P is nanofluid specific heat, T_i and T_o are the inlet and outlet temperatures of the collector, G_T is the incident radiative flux, and A_c is the collector area.

Therefore, the general uncertainty analysis to evaluate the thermal efficiency of the collector RSS leads to the following relationship:

$$U_\eta^2 = \left(\frac{\Delta(T_o - T_i)}{(T_o - T_i)}\right)^2 + \left(\frac{\Delta \dot{V}}{\dot{V}}\right)^2 + \left(\frac{\Delta G_T}{G_T}\right)^2. \tag{3}$$

The results for all tests were below 6%. The temperature sensors were calibrated using a calibrated thermometer to offer an uncertainty of less than $\pm 0.7^{\circ}$C; the calibration of the flowmeter was done by drawing off water from the system into a container and measuring the volume and time with accurate scales. The uncertainty was about $\pm 4\%$ and the intensity of incident radiation was recorded using a TES-1333 solar power meter that showed that uncertainty was about $\pm 5\%$.

2.3. Materials and preparation method

An improved Hummer method [41] was used in the preparation of the nanoparticles investigated in this study, including multi-layer GO nanoplates. At first, graphite powder (1.0 g) was dispersed in a mixture of concentrated (120 mL) H_2SO_4 and (13.5 mL) H_3PO_4 and then stirred for 24 hours. Then, $KMnO_4$ (6.0 g) was gradually added to the produced solution by continuous stirring at a temperature below 30°C. After 3 days of stirring the mixture and its cooling down to the room temperature, the reaction mixture was poured into 400 mL frozen water and 5 mL of H_2O_2 was subsequently added. The resulting suspension was washed by centrifugation with 10% HCl and then by water to remove residuals. The obtained graphite oxide was sonicated to achieve a stable GO dispersion in water. Finally, the resultant dispersion was subjected

Table 1. Non-Newtonian and Newtonian nanofluid samples with specifications of weight percentages and base fluids.

Nanofluid sample	Nano particle	Base fluid	Nano Particle Weight percentage
S_1	GO	Na-CMC 0.4%-DI	0.03%
S_2	GO	Na-CMC 0.4%-DI	0.01%
S_3	GO	DI	0.03%
S_4	GO	DI	0.01%
S_5	RGO	DI	0.03%
S_6	—	Na-CMC 0.4%-DI	—
S_7	—	DI	—

to the centrifugation process at 5000 rpm to remove the un-exfoliated graphite oxide. The purified GO was diluted by water to achieve 1 mgmL^{-1} GO dispersion for further use [42]. Also for RGO preparation, an amount of hydrazine hydrate was added into suspension and it was heated at 80°C for 24 h, and the weight ratio of hydrazine hydrate and GO was controlled at 10:7. A kind of black flocculent substance was gradually precipitated out of the solution. The product was obtained through filtration with high quality filter paper. Finally, the resulting black product was washed with methanol and water and dried at 80°C for 24 h. A two-step process was used to prepare nanofluid samples, namely adding GO nanoparticles to the base fluid depending on the weight percentages and then being dispersed completely in the fluid by magnetic mixing. In this study, the base fluid was selected for the Newtonian state of deionized water and for the non-Newtonian state of Na-CMC aqueous solution with the weight percentage of 0.4 wt%. Also, they have been prepared at weight percentages of 0.01 wt% and 0.03 wt% of GO for the testing process. It should be pointed out that the selected graphite flakes were purchased from Merck (99% carbon $< 44\ \mu$). Also, Na-CMC powder was purchased from Sigma-Aldrich (low viscosity). In accordance with similar researches, the weight percentages used this study were chosen for the preparation of dilute working fluid with low effective viscosity due to the need for low pumping power and long-term stability of nanoparticles. Since the stability of nanoparticles after the preparation of nanofluids is an important key concern, the stable suspension of nanofluid samples was provided for experimental testing in the collector using an ultrasonic bath apparatus for 1 hour. Experimental test samples of GO nanofluids are shown in Figure 2 based on the base fluid and weight percentages listed in Table 1.

Figure 2. Photographs of the nanofluids samples.

3. Properties of nanofluids

3.1. Viscosity

In this study, the viscosity of nanofluid samples has been measured by AntonPaar-CTD450 rheometer. The variation of shear stress and viscosity versus shear rates at the initial and final temperatures of the test, i.e. 20°C and 70°C, are shown in Figures 3 and 4, respectively. Additionally, the variation of viscosity versus temperature in shear rate 0.01 s^{-1} is indicated for non-Newtonian and Newtonian GO nanofluids in Figure 5.

The analytical results of the rheological behavior of non-Newtonian nanofluids at both weight percentage modes, based on the rheological nature of the nanofluid consisting of reference spherical nanoparticles [43], represented nanofluids with a shear-thinning (pseudo-plastic) non-Newtonian fluid behavior. The shear viscosity followed the Einstein equation and showed a relative increase by elevating weight percentage [44].

3.2. Specific heat

Specific heat is one of the important thermal properties of solar systems, which is directly related to thermal storage and transfer [45]. In nanofluids due to the presence of nanoparticles suspended in the base fluid, the surface area and thermal capacity of the fluid increase [8].

The specific heat of nanofluids is usually measured by Differential Scanning Calorimetry (DSC). In this study, the specific heat of nanofluid samples was measured by the DSC1 model (Mettler Toledo, Switzerland, according to ASTM E1269-18 standard in the test temperature range of 10°C to 90°C), it illustrated that the specific heat analysis in terms of temperature was as given in Figure 6 for research samples. The results showed that in the nanofluid GO with Newtonian base fluid, the specific heat experienced an ascending trend

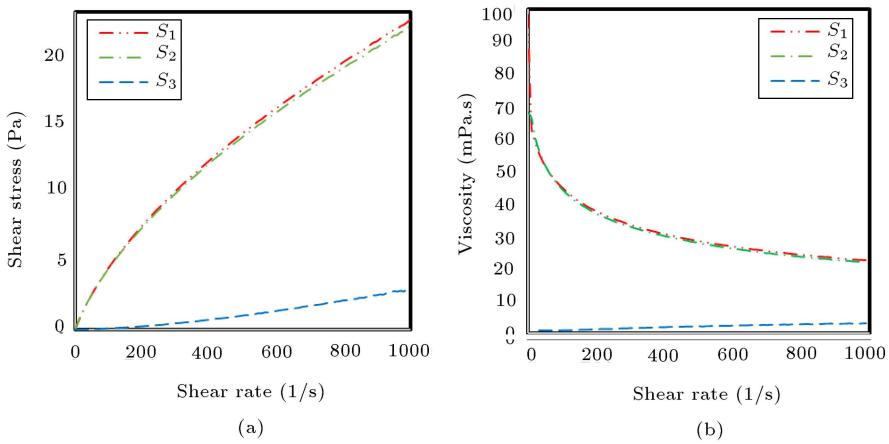

Figure 3. The variation of (a) shear stress and (b) viscosity versus shear rate for non-Newtonian and Newtonian Graphene Oxide (GO) nanofluids at 20°C.

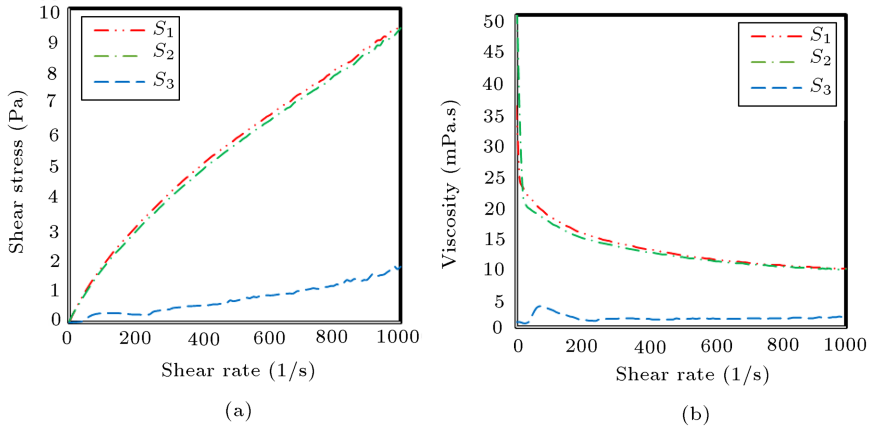

Figure 4. The variation of (a) shear stress and (b) viscosity versus shear rate for non-Newtonian and Newtonian Graphene Oxide (GO) nanofluids at 70°C.

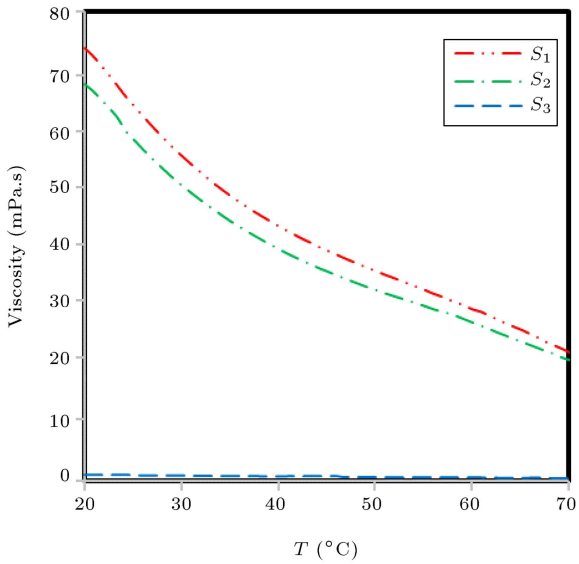

Figure 5. The variation of viscosity versus temperature in shear rate 0.01 s^{-1} for non-Newtonian and Newtonian Graphene Oxide (GO) nanofluids.

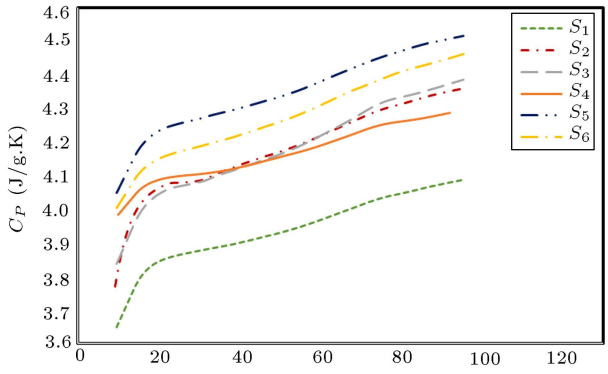

Figure 6. Effect of temperature on the specific heat of Graphene Oxide (GO) nanofluids.

by increasing weight percent. Moreover, in the GO nanofluid state based on non-Newtonian base fluid, this reverse trend was observed. Also, for both the Newtonian and non-Newtonian nanofluid states, there were specific heat changes with temperature in the ascending slope.

3.3. Radiative properties

By adding nanoparticles of different weight percentages, sizes, and types to the base fluid, the optical properties of the fluid, including absorption and scattering coefficients (generally known as extinction coefficient), were improved. This was vital to enhance the thermal efficiency of the thermal systems. It is worth noting that the contribution of each of these coefficients, depending on the type and conditions of the provided nanofluids, would affect the extinction coefficient. The effect of scattering is negligible if the nanoparticles diameter be less than 10 nm. Their effect will be more dominant as the particles size increases [46,47]. However, the effect of scattering can be also neglected when the particles volume fraction is less than 0.6% [48]. Furthermore, the scattering effect will be dramatically slight if the nanoparticles are far apart (well dispersed). In the present study, the absorbance of sample nanofluids was measured by a Specord 250 spectrometer. Since the volume fraction of samples is less than 0.1% [47] and the nanoparticles are well dispersed, so it is safe to assume working in the independent scattering regime which requires relatively simplistic optical properties calculations. The highest extinction coefficient (see Figure 7) was obtained for samples S_3 and S_1 for the Newtonian and non-Newtonian fluids, respectively.

4. Thermal performance of nanofluids

4.1. Collector thermal efficiency

General Collector efficiency (η) is the ratio of the useful energy to the total incident radiation on the collector surface:

$$\eta = \frac{\dot{Q}_u}{\dot{Q}_{\text{in}}}. \tag{4}$$

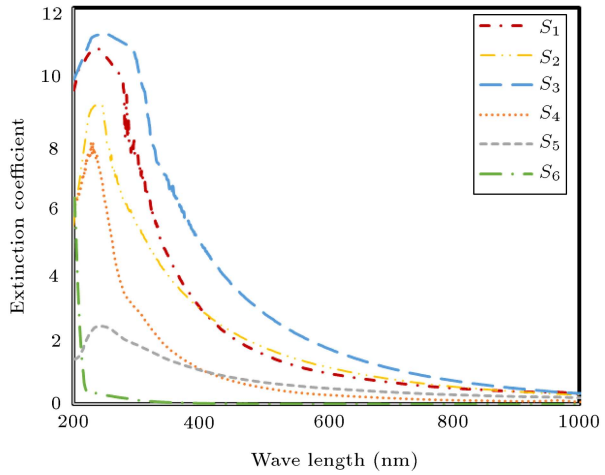

Figure 7. Extinction coefficient of sample nanofluids at different wavelengths.

The rate of useful energy of the collector can be expressed by using overall heat loss coefficient and the collector temperature as:

$$\dot{Q}_u = \dot{Q}_{\text{in}} - \dot{Q}_{\text{loss}} = [\tau\alpha G_T - U_L(T_c - T_{amb})]\, A_c. \tag{5}$$

Since it is difficult to define the collector average temperature in Eq. (4), it is convenient to define a quantity that relates the ratio of the heat actually delivered by the collector to the heat. The latter will be delivered if the whole collector surface be at the fluid inlet temperature [49]. This quantity is known as "the collector heat removal factor (F_R)" and is expressed by:

$$F_R = \frac{\rho\dot{V}C_P(T_o - T_i)}{[\tau\alpha G_T - U_L(T_i - T_{amb})]\, A_c}. \tag{6}$$

By inserting Eqs. (5) and (6) in Eq. (4), the instantaneous efficiency of the collector is obtained by the following relation:

$$\eta = F_R(\tau\alpha) - F_R U_L T^*. \tag{7}$$

This relation indicates the dependence of the thermal efficiency on the three parameters. $F_R(\tau\alpha)$ stands for the maximum collector efficiency and zero efficiency is denoted by (η_0) at which the inlet temperature reaches ambient temperature. Also, $F_R U_L$ is the energy dissipation coefficient and $T^* = (T_i - T_{amb})/G_T$ which represents the decreasing temperature difference. Since, firstly HQI 1000 W/D Osram lamp has a color temperature of 7250 K, which has remarkably higher irradiation intensity at UV bands comparing to the incident solar radiation. Secondly, the tested nanofluids have high extinction peaks at UV bands. Therefore, the obtained efficiencies in this study are expected to be higher than those obtained under solar irradiation for the same nanofluids and same weight percentage.

4.2. Indicator of the temperature difference rise rate

After the collector model system reached the steady-state mode, an index was defined to estimate the trend of increasing temperature difference rate affected by test parameters such as change of base fluid from Newtonian to non-Newtonian, weight percentage, volume flow rate, and incident radiative flux. This index was used to evaluate the difference between the average temperature inside the collector chamber and the collector inlet temperature for the nanofluid samples in the initial test time (after reaching the steady-state mode) and after 15 minutes under the same conditions, as given below:

$$A = \frac{(T_{mf} - T_{if}) - (T_{m0} - T_{i0})}{\Delta t_{0-f}}. \tag{8}$$

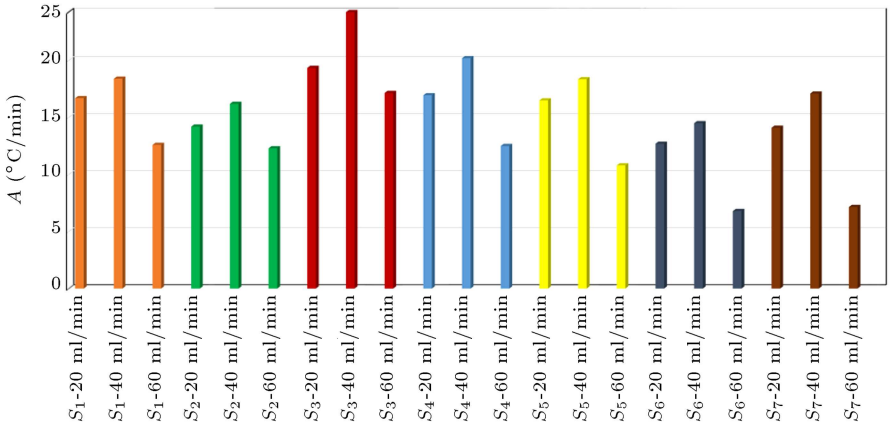

Figure 8. Indicator of the temperature difference rise rate of the Direct Absorption Solar Collector (DASC) in the test period.

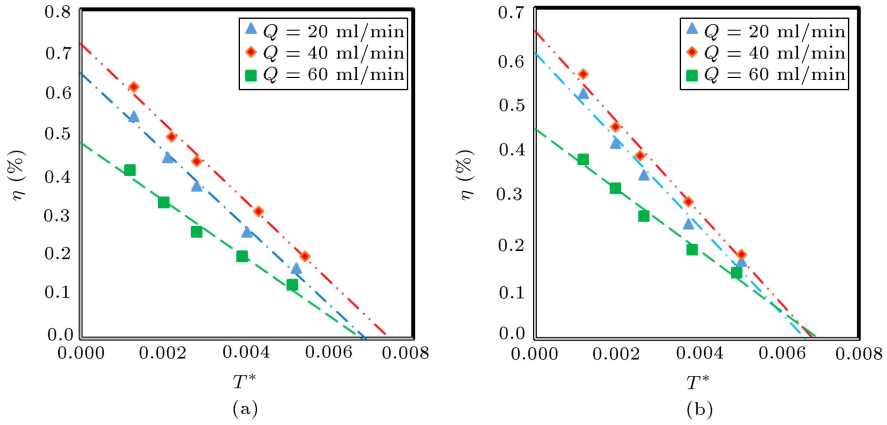

Figure 9. Effect of reduced temperature difference on collector efficiency for (a) S_1 sample and (b) S_2 sample nanofluid, at various volume flow rates.

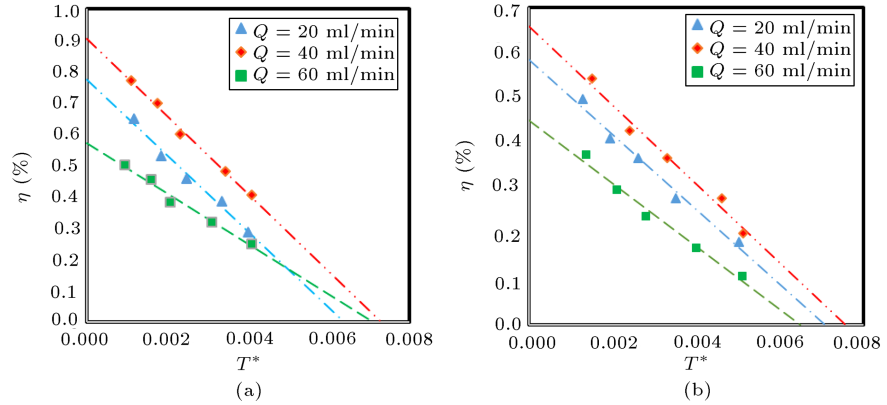

Figure 10. Effect of reduced temperature difference on collector efficiency for (a) S_3 sample and (b) S_4 sample nanofluid at various volume flow rates.

This illustrates that the estimation results (see Figure 8) represent the largest quantity for S_3 nanofluid sample with a volume flow rate of 40 ml/min. Indicator A is in contrast to the efficiency of a dimensional quantity in (°C/min), illustrating the rate of increase in the temperature difference of the direct absorption collector model.

5. Result and discussion

The obtained results regarding the effect of volume flow rate on the thermal efficiency relative to the decreasing temperature difference in the low-temperature DASC (according to Figures 9–11) implies that a change in the volume flow rate from 20 to 40 ml/min causes an

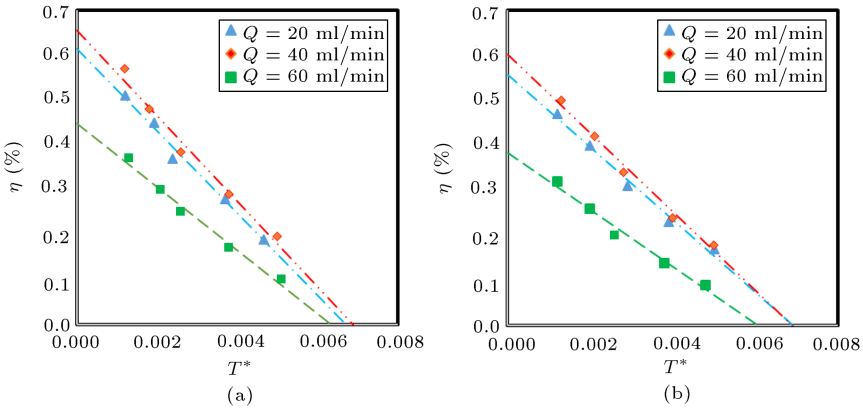

Figure 11. Effect of reduced temperature difference on collector efficiency for (a) S_5 sample and (b) S_6 sample nanofluid, at various volume flow rates.

increase in the thermal efficiency. Here, the curve slope has not been tangibly varied and, in turn, $F_R U_L$ has remained constant according to Eq. (7) whereas the y-intercept (η_0) has been augmented which shows the enlargement of F_R, i.e. the received heat by radiation (Eqs. (6)) has increased which is due to the escalation of passing fluid volume rate per time unit. A general examination of curves suggested that the thermal efficiency of the collector is higher for deionized water as the base fluid compared to Na-CMC. In this regard, a comparison of Figures 9 and 10 demonstrated that the effect of a fluid flow rate increase from 20 to 40 ml/min on the thermal efficiency has been higher for deionized water as the base fluid which can be attributed to higher thermal radiation absorption (Figure 7) and specific heat (Figure 6) compared to similar states. Furthermore, Figures 9 and 10 reveals that the effect of the flow rate increase on the thermal efficiency has been higher for nanoparticles with larger weight percentages in both nanofluids with deionized water and Na-CMC base fluids, which is due to immense thermal radiation absorption for both Newtonian and non-Newtonian nanofluids (Figure 7). The thermal efficiency ascended by increasing the volume flow rate to 60 ml/min which might be due to the decrease in the heat removal factor F_R and increase in the heat loss U_L. Despite the augmentation of volume flow rate, the slope of lines and thermal efficiency are reduced compared to the two previous test volumetric flow rates. The results (Figure 11(a)) for the nanofluid S_5 sample (RGO) have a qualitative trend identical to that of S_2 and S_4 samples. However, from a quantitative standpoint, the loss of efficiency is observed at all of the three test flow rates due to the lower thermal radiation absorption. Figure 11(b) shows the effect of the volume flow rate on the thermal efficiency of the non-Newtonian base fluid S_6 (Na-CMC), indicating a thermal efficiency loss (6.84–22.23%) compared to the deionized water base fluid where the loss trend is ascending with flow rate increase. Finally, the overall assessment of the effect of volume flow rate on the test samples suggested the optimum flow rate of 40 ml/min yielding the maximum thermal efficiency in different modes of experiments.

Figures 12–14 depict the effect of changing collector working fluid from Newtonian to non-Newtonian

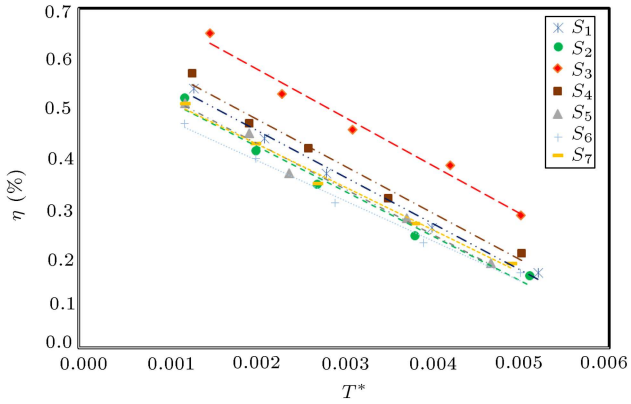

Figure 12. Effect of working fluid change from Newtonian to non-Newtonian fluid on collector efficiency at the flow rate of 20 ml/min.

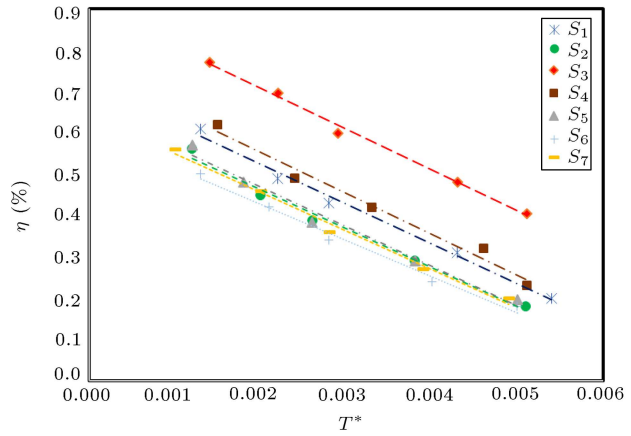

Figure 13. Effect of working fluid change from Newtonian to non-Newtonian fluid on collector efficiency at the flow rate of 40 ml/min.

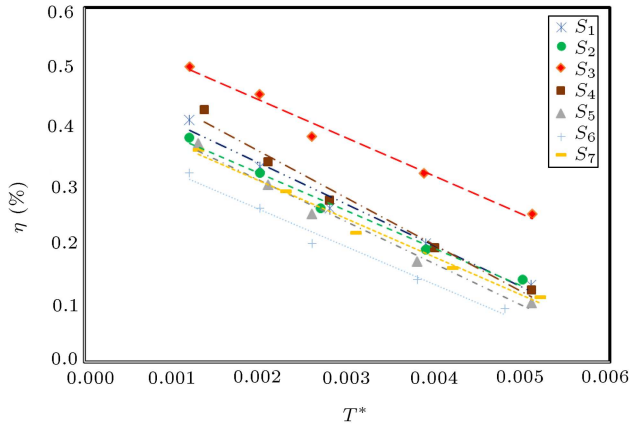

Figure 14. Effect of working fluid change from Newtonian to non-Newtonian fluid on collector efficiency at the flow rate of 60 ml/min.

and variation in the weight percentage on the collector thermal efficiency. As can be observed, as the weight percentage increased from 0.01 wt% to 0.03 wt% in the GO nanofluid with Newtonian base fluid (deionized water), the thermal efficiency enlarged from 11.4 to 36.19%, whereas this trend was milder (from 3.84 to 11.12%) for the GO nanofluid with non-Newtonian base fluid Na-CMC which might be due to higher thermal absorption attributable to the increase in the weight percentage from 0.01 to 0.03 wt% in both Newtonian and non-Newtonian modes (Figure 7). Moreover, altering the working fluid from the Newtonian to non-Newtonian mode at the same weight percentage led to the reduction of thermal efficiency (9.4–15.63% at the weight percentage of 0.01 wt% and 19.84–26.46% at the weight percentage of 0.03 wt%), which is owing to lower specific heat C_p (Figure 6) and less thermal radiation absorption (Figure 7) in the non-Newtonian mode. The comparison of the RGO nanofluid with Newtonian/non-Newtonian graphene nanofluids at 0.03 wt% showed the efficiency loss, which might be attributed to the absorption decrease in the RGO. The results of the overall heat loss coefficients and zero-loss efficiencies for the tested nanofluid samples are shown in Table 2.

6. Conclusion

The present study focused on two factors influencing Graphene Oxide (GO) nanofluids –the specific advantages and thermal potential of non-Newtonian nanofluids– to improve the thermal performance of Direct Absorption Solar Collectors (DASCs). The obtained results are summarized as follows:

- GO nanofluid at 0.03 wt% in both Newtonian and non-Newtonian states has offered a strong absorption wavelength range of 230 to 300 nm, which has been a good choice for DASC;

Table 2. R-squared values (coefficient of determination), zero-loss efficiencies and heat loss coefficients for non-Newtonian and Newtonian working fluids at various volume flow rates.

Nanofluid sample	Flow rate range (ml/min)	$F_R U_L$	η_0	R^2
S_1	20	93.884	0.645	0.991
	40	96.118	0.715	0.99
	60	70.211	0.476	0.981
S_2	20	90.369	0.606	0.98
	40	94.663	0.652	0.987
	60	63.447	0.445	0.986
S_3	20	96.784	0.773	0.98
	40	98.875	0.905	0.995
	60	64.403	0.572	0.982
S_4	20	94.382	0.668	0.983
	40	99.597	0.753	0.981
	60	79.53	0.515	0.982
S_5	20	91.475	0.614	0.986
	40	95.565	0.659	0.98
	60	70.633	0.448	0.986
S_6	20	80.574	0.557	0.988
	40	87.403	0.601	0.988
	60	63.45	0.385	0.981

- Increasing the weight percentage from 0.01 wt% to 0.03 wt% has improved the temperature difference rise rate index and has resulted in a comparative increase in collector thermal efficiency in both Newtonian and non-Newtonian fluids by 11.4–36.19% and 3.84–11.12% relative to the base fluid, respectively;
- As fluid converted from Newtonian to non-Newtonian mode, the thermal efficiency of the collector was reduced, resulting in the weight percentage of 0.03 with a steeper slope in the range of 19.84% to 26.46% under test conditions;
- By evaluating the effect of volume flow rate on the thermal performance of the designed model for 5 nanofluid samples and test weight percentages the most optimal results at the volume flow rate of 40 ml/min was revealed. This implies that the increase in volume flow rate to 40 ml/min has diminished nanofluid thermal absorption power;
- The results of the comparison between thermal

efficiency and temperature difference rise rate for GO and Reduced Graphene Oxide (RGO) nanofluids at the same weight percentage revealed a marked decrease in efficiency for the RGO state;

- By comparing the three indices in terms of optical properties improvement, thermal efficiency of collector, and temperature rise rate in the designed direct absorption collector model the appropriate results were obtained for nanofluid samples. As the results showed, the most desirable option has been the nanofluid of sample S_3 with a flow rate of 40 ml/min.

Nomenclature

A	Temperature difference rise rate ($^\circ$C.min^{-1})
A_c	Top surface area of the collector (m^2)
C_P	Specific heat (J.kg^{-1}$^\circ$C^{-1})
F_R	Collector heat removal factor (–)
G_T	Total incident radiative flux (W.m^{-2})
$\dot{Q}_{\text{in}}$	Rate of total received energy (W)
$\dot{Q}_{\text{loss}}$	Rate of loss energy (W)
$\dot{Q}_u$	Rate of useful energy (W)
R	Coefficient of determination (–)
S	Nanofluid sample (–)
T_{amb}	Ambient temperature ($^\circ$C)
T_c	Collector temperature ($^\circ$C)
T_i	Inlet fluid temperature ($^\circ$C)
T_{i0}	Inlet temperature in initial time ($^\circ$C)
T_{if}	Inlet temperature in final time ($^\circ$C)
T_{m0}	Mean temperature in initial time ($^\circ$C)
T_{mf}	Mean temperature in final time ($^\circ$C)
T_o	Outlet fluid temperature ($^\circ$C)
T^*	Reduced temperature difference ($^\circ$C.m^2.W^{-1})
U_L	Overall heat loss coefficient (W.m^{-2}$^\circ$C^{-1})
U_r	General uncertainty (%)
U_{xj}	Component uncertainty (%)
U_η	Efficiency uncertainty (%)
$\dot{V}$	Volume flow rate (m^3.s^{-1})
Δt	Test time (min)

Greek symbols

α	Absorbance (%)
τ	Transmittance (%)
η	Instantaneous collector efficiency (%)
η_0	Zero-loss collector efficiency (%)
λ	Wave length (μm)
ρ	Density (kg.m^{-3})

References

1. Modest, M.F., *Radiative Heat Transfer*, The University of California at Merced, 3th Edn, Academic Press is an imprint of Elsevier (2013).
2. Timofeeva, E.V., *Nanofluids for Heat Transfer Potential and Engineering Strategies*, Energy Systems Division, Argonne National Laboratory, Argonne, IL USA, **19**, pp. 435–446 (2011).
3. Duffie, J.A. and Beckman, W.A., *Solar Engineering of Thermal Processes*, Published by John Wiley & Sons, Inc., Hoboken (2013).
4. Li, Z.X. and Khaled, U., Al-Rashed, A.A., Goodarzi, M., Sarafraz, M.M., and Meer, R. "Heat transfer evaluation of a micro heat exchanger cooling with spherical carbon-acetone nanofluid", *International Journal of Heat and Mass Transfer*, **149**, pp. 119–124 (2020).
5. Sheikholeslami, M., Rezaeianjouybari, B., Darzi, M., Shafee, A., Li, Z., and Nguyen, T.K. "Application of nano-refrigerant for boiling heat transfer enhancement employing an experimental study", *International Journal of Heat and Mass Transfer*, **141**, pp. 974–980 (2019).
6. Elsheikh, A.H., Sharshir, S.W., Mostafa, M.E., Essa, F.A., and Ahmed Ali, M.K. "Applications of nanofluids in solar energy: A review of recent advances", *Renewable and Sustainable Energy Reviews*, **82**(3), pp. 3483–3502 (2018).
7. Sharma, K. and Kundan, L. "Nanofluid Based Concentrating Parabolic Solar Collector (NBCPSC): A new alternative", *International Journal of Research in Mechanical Engineering & Technology*, **4**(2), pp. 146–152 (2014).
8. Xuan, Y. and Li, Q. "Heat transfer enhancement of nanofluids", *International Journal of Heat and Fluid Flow*, **21**(1), pp. 58–64 (2000).
9. Standard, A. "Standard tables for reference solar spectral irradiances: Direct normal and hemispherical on 37 tilted surface", *Amer. Society for Testing Matls.*, West Conshocken PA, USA, G173 (2007).
10. Mallah, A.R., Mohd Zubir, M.N., Alawi, O.A., Newaz, K.S., and Badry, A.B. "Plasmonic nanofluids for high photothermal conversion efficiency in direct absorption solar collectors: Fundamentals and applications", *Solar Energy Materials and Solar Cells*, **201**, pp. 1–31 (2019).
11. Sadeghinezhad, E., Mehrali, M., Saidur, R., Mehrali, Me. Latibari, S.T., Akhiani, A., and Metselaar, H.S.C. "A comprehensive review on graphene nanofluids: Recent research, development and applications", *Energy Conversion and Management*, **111**, pp. 466–487 (2016).

12. Minardi, J.E. and Chuang, H.N. "Performance of a "black" liquid flat-plate solar collector", *Solar Energy*, **17**, pp. 179–183 (1975).

13. Luo, Z., Wang, C., Wei, W., Xiao, G., and Ni, M. "Performance improvement of a nanofluid solar collector based on direct absorption collection (DAC) concepts", *International Journal of Heat and Mass Transfer*, **75**, pp. 262–271 (2014).

14. Liu, J., Ye, Z., Zhang, L., Fang, X., and Zhang, Z. "A combined numerical and experimental study on graphene/ionic liquid nanofluid based direct absorption solar collector", *Solar Energy Materials & Solar Cells*, **136**, pp. 177–186 (2015).

15. Vakili, M., Hosseinalipour, S.M., Delfani, S., Khosrojerdi, S., and Karami, M. "Experimental investigation of graphene nanoplatelets nanofluid-based volumetric solar collector for domestic hot water systems", *Solar Energy*, **131**, pp. 119–130 (2016).

16. Vakili, M., Hosseinalipour, S.M., Delfani, S., and Khosrojerdi, S. "Photo- thermal properties of graphene nanoplatelets nanofluid for low-temperature direct absorption solar collectors", *Solar Energy Materials & Solar Cells*, **152**, pp. 187–191 (2016).

17. Khosrojerdi, S., Lavasani, A.M., and Vakili, M. "Experimental study of photo-thermal specifications and stability of graphene oxide nanoplatelets nanofluid as working fluid for low-temperature Direct Absorption Solar Collectors (DASCs)", *Solar Energy Materials & Solar Cells*, **164**, pp. 32–39 (2017).

18. Chen, L., Liu, J., Fang, X., and Zhang, Z. "Reduced graphene oxide dispersed nanofluids with improved photo-thermal conversion performance for direct absorption solar collectors", *Solar Energy Materials & Solar Cells*, **163**, pp. 125–133 (2017).

19. Ma, X., Liua, Y., Liua, H., Zhanga, L., Xua, B., and Xiaob, F. "Fabrication of novel slurry containing graphene oxide-modified microencapsulated phase change material for direct absorption solar collector", *Solar Energy Materials and Solar Cells*, **188**, pp. 73–80 (2018).

20. Campos, C., Vasco, D., Angulo, C., Burdiles, P.A., Cardemilc, J., and Palzaa, H. "About the relevance of particle shape and graphene oxide on the behavior of direct absorption solar collectors using metal based nanofluids under different radiation intensities", *Energy Conversion and Management*, **181**, pp. 247–257 (2019).

21. Xu, X., Xu, C., Liu, J., Fang, X., and Zhang, Z. "A direct absorption solar collector based on a water-ethylene glycol based nanofluid with anti-freeze property and excellent dispersion stability", *Renewable Energy*, **133**, pp. 760–769 (2019).

22. Gorji, T.B. and Ranjbar, A.A. "A review on optical properties and application of nanofluids in direct absorption solar collectors (DASCs)", *Renewable and Sustainable Energy Reviews*, **72**, pp. 10–32 (2017).

23. Wang, D., Jia, Y., He, Y., Wang, L., Fan, J., Xie, H., and Yu, W. "Enhanced photo thermal conversion properties of magnetic nanofluids through rotating magnetic field for direct absorption solar collector", *Journal of Colloid and Interface Science*, **557**, pp. 266–275 (2019).

24. Wang, D., Jia, Y., He, Y., Wang, L., Xie, H., and Yu, W. "Photo thermal efficiency enhancement of a nanofluid-based direct absorption solar collector utilizing magnetic nano-rotor", *Energy Conversion and Management*, **199**, p. 111996 (2019).

25. Huang, J., Chen, Z., Du, Z., Xu, X., Zhang, Z., and Fang, X. "A highly stable hydroxylated graphene/ethylene glycol-water nanofluid with excellent extinction property at a low loading for direct absorption solar collectors", *Thermochimica Acta*, **684**, p. 178487 (2020).

26. Sharaf, O.Z., Rizk, N., Joshi, C.P., Jaoudé, M.A., Al-Khateeb, A.N., Kyritsis, D.C., Abu-Nada, E., and Martinc, M.N. "Ultrastable plasmonic nanofluids in optimized direct absorption solar collectors", *Energy Conversion and Management*, **199**, p. 112010 (2019).

27. Hazra, S.K., Ghosh, S., and Nandi, T.K. "Photo-thermal conversion characteristics of carbon black-ethylene glycol nanofluids for applications in direct absorption solar collectors", *Applied Thermal Engineering*, **163**, p. 114402 (2019).

28. Wang, K., He, Y., Kan, A., Yu, W., Wang, D., Zhang, L., Zhu, G., Xie, H., and She, X. "Significant photo thermal conversion enhancement of nanofluids induced by Rayleigh-Bénard convection for direct absorption solar collectors", *Applied Energy*, **254**, p. 113706 (2019).

29. Delfani, S., Esmaeili, M., and Karami, M. "Application of artificial neural network for performance prediction of a nanofluid-based direct absorption solar collector", *Sustainable Energy Technologies and Assessments*, **36**, p. 100559 (2019).

30. Wang, Z., Qu, J., Zhang, R., Han, X., and Wu, J. "Photo-thermal performance evaluation on MWCNTs-dispersed microencapsulated PCM slurries for direct absorption solar collectors", *Journal of Energy Storage*, **26**, p. 100793 (2019).

31. Li, B., Lin, Y., Zhu, L., and Zhang, W. "Effects of non-Newtonian behavior on the thermal performance of nanofluids in a horizontal channel with discrete regions of heating and cooling", *Applied Thermal Engineering*, **94**, pp. 404–412 (2015).

32. Hojjat, M., Etemad, S.Gh., Bagheri, R., and Thibault, J. "Thermal conductivity of non-Newtonian nanofluids: Experimental data and modeling using neural network", *International Journal of Heat and Mass Transfer*, **54**(6), pp. 1017–1023 (2011).

33. Pimenta, T.A. and Campos, J.B.L.M. "Heat transfer coefficients from Newtonian and non-Newtonian fluids flowing in laminar regime in a helical coil", *International Journal of Heat and Mass Transfer*, **58**(2), pp. 676–690 (2013).

34. Sharifi Asl, M., Toghraei, D.A., and Azimian, R. "Numerical investigation on heat transfer coefficient enhancement of non-Newtonian nanofluid in the turbulent flow inside a tube", *Indian J. Sci. Res.*, **1**(2), pp. 363–369 (2014).

35. Akbari, O.A., Toghraie, D., Karimipourc, A., Marzband, A., and Ahmadi, Gh.R. "The effect of velocity and dimension of solid nanoparticles on heat transfer in non-Newtonian nanofluid", *Physica E*, **86**, pp. 68–75 (2017).

36. Shamsi, M.R., Ali Akbari, O., Marzban, A., Toghraie, D., and Mashayekhi, R. "Increasing heat transfer of non-Newtonian nanofluid in rectangular microchannel with triangular ribs", *Physica E*, **93**, pp. 167–178 (2017).

37. Shahsavani, E., Afrand, M., and Kalbasi, R. "Using experimental data to estimate the heat transfer and pressure drop of non-Newtonian nanofluid flow through a circular tube: Applicable for use in heat exchangers", *Applied Thermal Engineering*, **129**, pp. 1573–1581 (2018).

38. Siddiqa, S., Begum, N., Hossain, A., Shoaib, M., and Gorla, R.S.R. "Radiative heat transfer analysis of non-Newtonian dusty Casson fluid flow along a complex wavy surface", *Numerical Heat Transfer, Part A: Applications, an International Journal of Computation and Methodology*, **73**(4), pp. 209–221 (2017).

39. Gorji, T.B. and Ranjbar, A.A. "A numerical and experimental investigation on the performance of a low-flux direct absorption solar collector (DASC) using graphite, magnetite and silver nanofluids", *Solar Energy*, **135**, pp. 493–505 (2016).

40. Moffat, R.J. "Describing the uncertainties in experimental results", *Experimental Thermal and Fluid Science*, **1**(1), pp. 3–17 (1988).

41. Marcano, D.C., Kosynkin, D.V., Berlin, J.M., Sinitskii, A., Sun, Z., Slesarev, A., Alemany, L.B., Lu, W., and Tour, J.M. "Improved synthesis of graphene oxide", *ACS Nano*, **4**(8), pp. 4806–4814 (2010).

42. Tabrizi, A.G., Arsalani, N., Namazi, H., and Ahadzadeh, I. "Vanadium oxide assisted synthesis of polyaniline nanoarrays on graphene oxide sheets and its application in super capacitors", *Journal of Electroanalytical Chemistry*, **798**, pp. 34–41 (2017).

43. Chen, H., Ding, Y., and Tan, C. "Rheological behavior of nanofluids", *New J. Phys.*, **9**(10), pp. 367–367 (2007).

44. Einstein, A. "Correction of my Work: A new determination of the molecular dimensions", *Ann. Phys.*, **34**(3), pp. 591–592 (1911).

45. Prasad, A.R., Singh, S., and Nagar, H. "A review on nanofluids: Properties and applications", *International Journal of Advance Research and Innovative Ideas in Education*, **3**(3), pp. 3185–3209 (2017).

46. Noguez, C. "Optical properties of isolated and supported metal nanoparticles", *Optical Materials*, **27**(7), pp. 1204–1211 (2005).

47. Taylor, R.A., Otanicar, T., and Rosengarten, G. "Nanofluid-based optical filter optimization for PV/T systems", *Science & Applications*, **1**(34), pp. 1–7 (2012).

48. Taylor, R.A., Phelan, P.E., Otanicar, T.P., Adrian, R., and Prasher, R. "Nanofluid optical property characterization: towards efficient direct absorption solar collectors", *Nanoscale Res Lett*, **6**(1), p. 225 (2011).

49. Struckmann, F. "Analysis of flat plate solar collector", Project Report MVK 160, Lund, Sweden, Heat and Mass Transport (2008).

Biographies

Vahid Sadeghi is a PhD candidate of Mechanical Engineering at the University of Tabriz. His research interests include nanofluids and their application in solar systems, renewable energy, radiation heat transfer, and fluid mechanics.

Sima Baheri Islami received her BSc degree in 1999 in Mechanical Engineering and MSc degree in 2002 in Thermo-Fluid Engineering, both from the University of Tabriz, Tabriz, Iran. She is a graduate of the University of Tabriz with a PhD in Thermo-Fluid Engineering. She started her academic position at the University of Tabriz as an Assistant Professor in 2009. Currently, she is an Associate Professor of Thermo-Fluid Engineering at Faculty of Mechanical Engineering, University of Tabriz, Iran. Her research fields are non-Newtonian fluids, computational fluid dynamics, convective heat transfer, micromixers, and lab-on-a-chip.

Nasser Arsalani was born in 1965 in Torbatejam, Iran. He obtained his BSc degree in Chemistry from the University of Tabriz in 1989 and MSc degree in Organic Chemistry from the University of Tabriz with Professor Ali Entezami as a supervisor in 1991. He worked as a lecture in the Organic Chemistry Department for two years from 1991 till 1993. After that, he received his PhD under the supervision of Professor Kurt E. Geckeler in 1997 from the University of Karls Eberhardt, Tuebingen, Germany. He joined again the Organic Chemistry Department of the University of Tabriz in 1997. His research field involves the synthesis of various new nano compounds, especially in the synthesis of nanobiomaterials, conducting polymers, nano catalysts, super capacitors, and drug delivery. He has published more than 95 research articles, 2 books, and one patent. He has also presented over 75 papers in domestic and foreign conferences and symposiums.